Supporting Information

pH-dependent formation of different coordination cages based on Co_4-TC4A secondary building units and bridging ligands

Xinxin Hang[a, b], Shentang Wang[a, b], Xiaofei Zhu[a], Haitao Han[a, b], Wuping Liao[a, *]

[a]State Key Laboratory of Rare Earth Resource Utilization, ERC for the Separation and Purification of REs and Thorium, Changchun Institute of Applied Chemistry, Chinese Academy of Sciences, Changchun 130022, China.

[b]University of Chinese Academy of Sciences, Beijing, 100049, China.

The SQUEEZE results for CIAC-117-CIAC-120

The disordered solvent molecules and counter cations in the voids in/between the cages cannot be located from Difference Fourier maps. Therefore, the data were treated by PLATON/SQUEEZE to estimate the contribution of these disordered groups [1].

SQUEEZE results for these four compounds are as follows:

(1) CIAC-117

```
loop_
   _platon_squeeze_void_nr
   _platon_squeeze_void_average_x
   _platon_squeeze_void_average_y
   _platon_squeeze_void_average_z
   _platon_squeeze_void_volume
   _platon_squeeze_void_count_electrons
   _platon_squeeze_void_content
    1 -0.008 0.000 -0.009         19197          5446 ' '
```

(2) CIAC-118

```
loop_
   _platon_squeeze_void_nr
   _platon_squeeze_void_average_x
   _platon_squeeze_void_average_y
   _platon_squeeze_void_average_z
   _platon_squeeze_void_volume
   _platon_squeeze_void_count_electrons
   _platon_squeeze_void_content
    1   0.000   0.000   0.000            10            15 ' '
    2   0.000   0.000   0.500           772           298 ' '
    3 -0.049   0.247 -0.081          7523          2368 ' '
    4   0.500   0.500   0.000           772           298 ' '
    5   0.500   0.500   0.500            10            15 ' '
```

(3) CIAC-119

```
loop_
   _platon_squeeze_void_nr
   _platon_squeeze_void_average_x
   _platon_squeeze_void_average_y
   _platon_squeeze_void_average_z
   _platon_squeeze_void_volume
   _platon_squeeze_void_count_electrons
   _platon_squeeze_void_content
    1 -0.005   0.000 -0.005         15881          4778 ' '
```

(4) CIAC-120

```
loop_
   _platon_squeeze_void_nr
   _platon_squeeze_void_average_x
```

_platon_squeeze_void_average_y
_platon_squeeze_void_average_z
_platon_squeeze_void_volume
_platon_squeeze_void_count_electrons
_platon_squeeze_void_content

1	0.000	0.000	0.000	819	221 ' '
2	0.000	0.000	0.500	23	0 ' '
3	-0.050	0.254	0.424	7083	1323 ' '
4	0.500	0.500	0.500	819	221 ' '
5	0.500	0.500	0.000	23	0 ' '

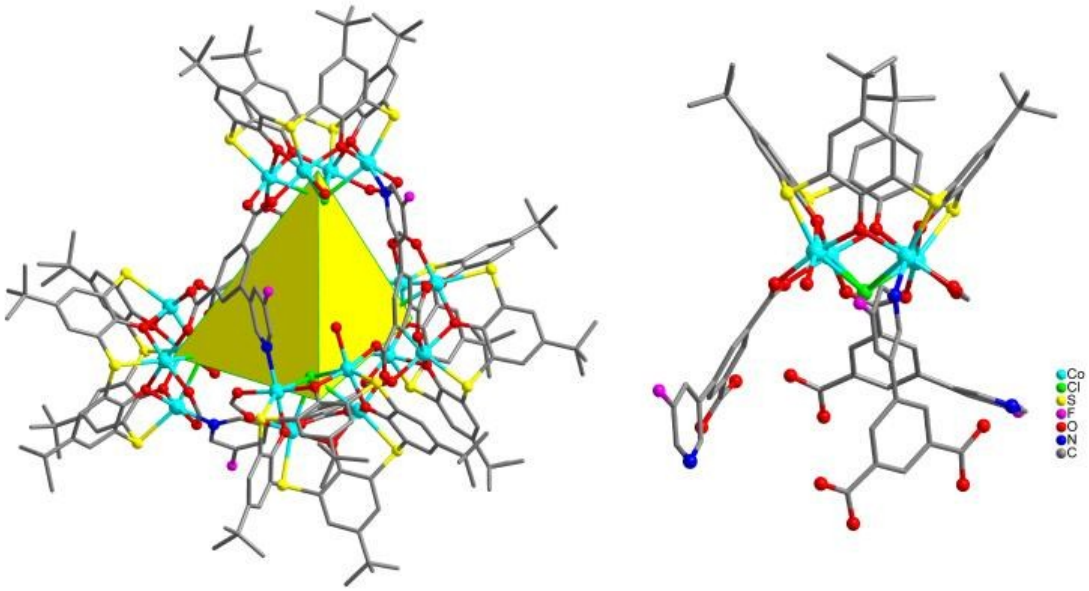

Fig. S1. Molecular structure of cage **CIAC-119** (left) as well as connection modes of the shuttlecock-like SBU (right).

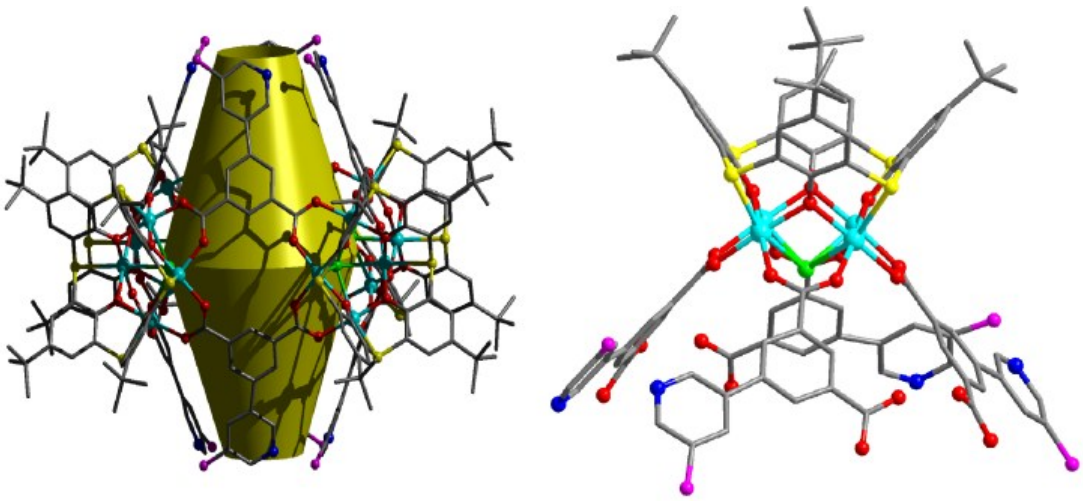

Fig. S2. Molecular structure of cage **CIAC-120** (left) as well as connection modes of the shuttlecock-like SBU (right).

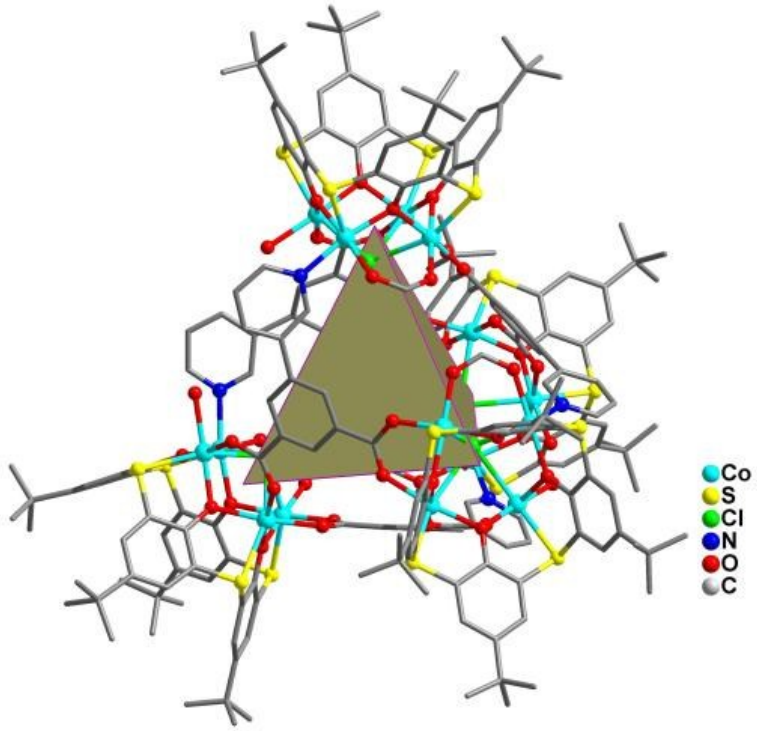

Fig. S3 Six portals on the edge of the facet-capped tetrahedron **CIAC-117**.

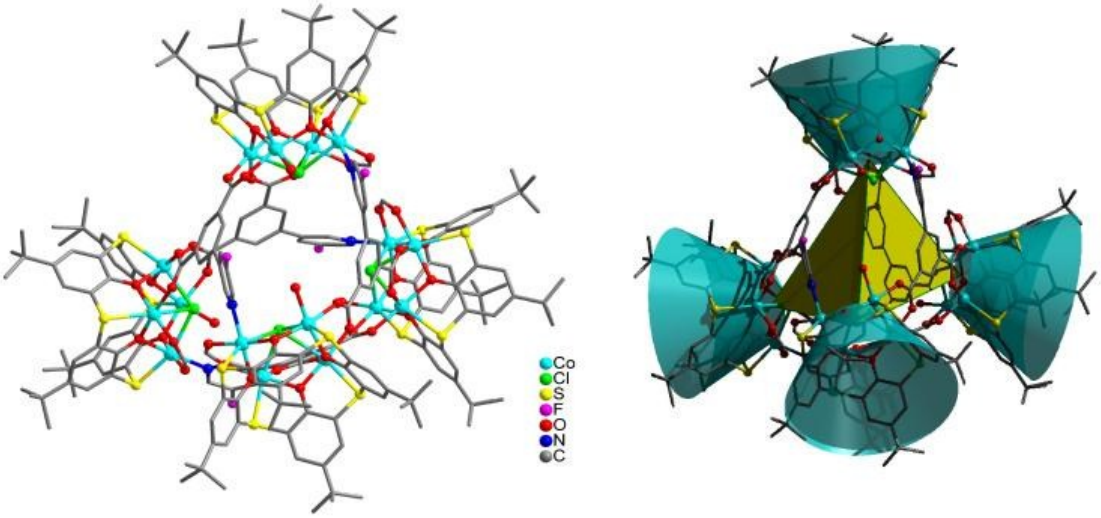

Fig. S4 Molecular structure of **CIAC-119**.

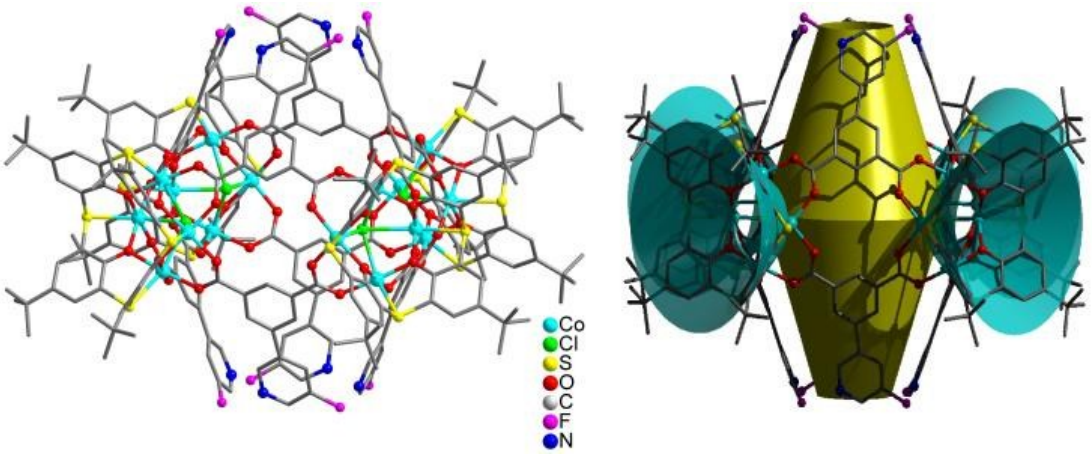

Fig. S5 Molecular structure of **CIAC-120**.

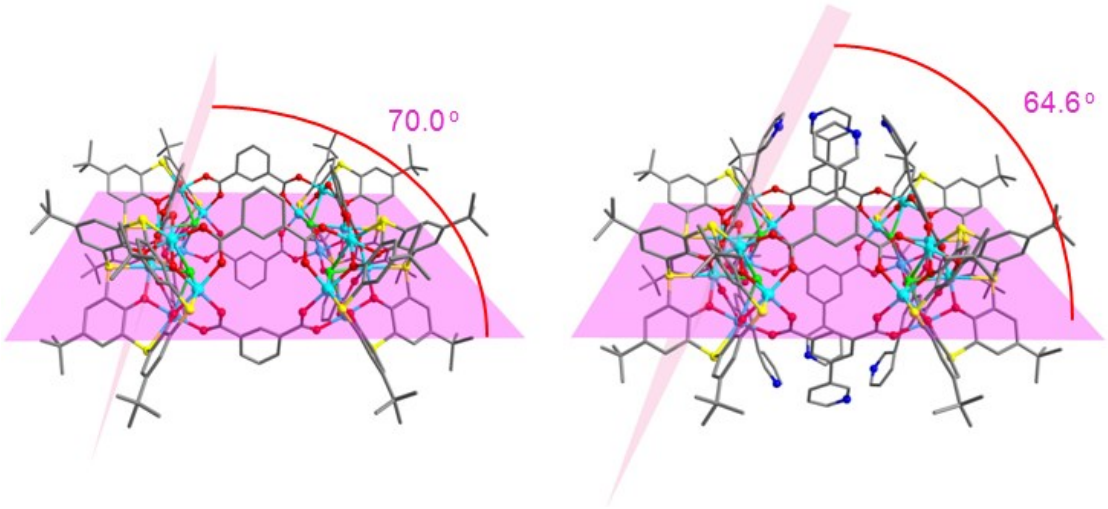

Fig. S6. Comparison of molecular structures of **CIAC-201**(left) and **CIAC-118** (right).

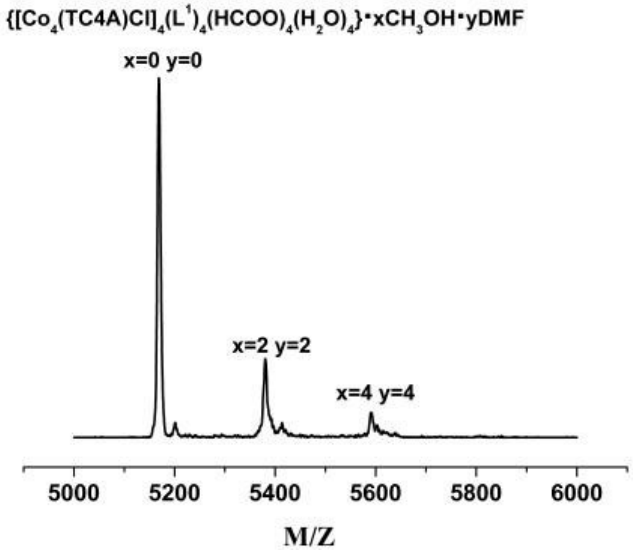

Fig. S7. MALDI-TOF mass spectrum of the resulting solutions presenting the feature peaks of $\{[Co_4(TC4A)Cl]_4(L^1)_4(HCOO)_4(H_2O)_4\}$ assembly in **CIAC-117**.

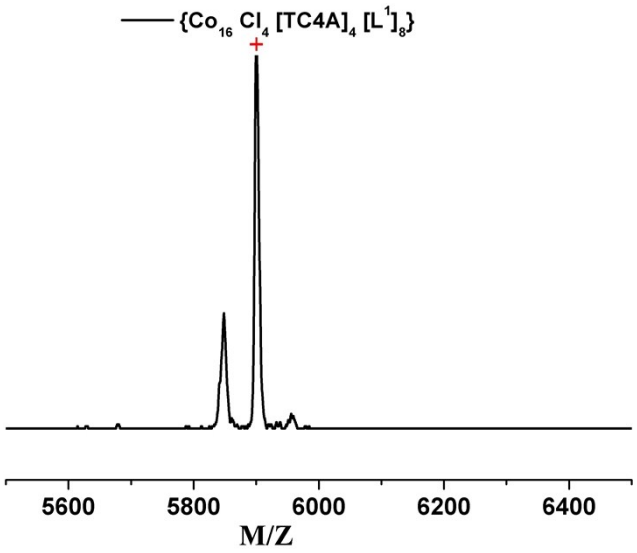

Fig. S8. MALDI-TOF mass spectrum of the resulting solutions presenting the feature peaks of $\{[Co_{16}Cl_4[TC4A]_4[L^1]_8\}$ assembly in **CIAC-118**.

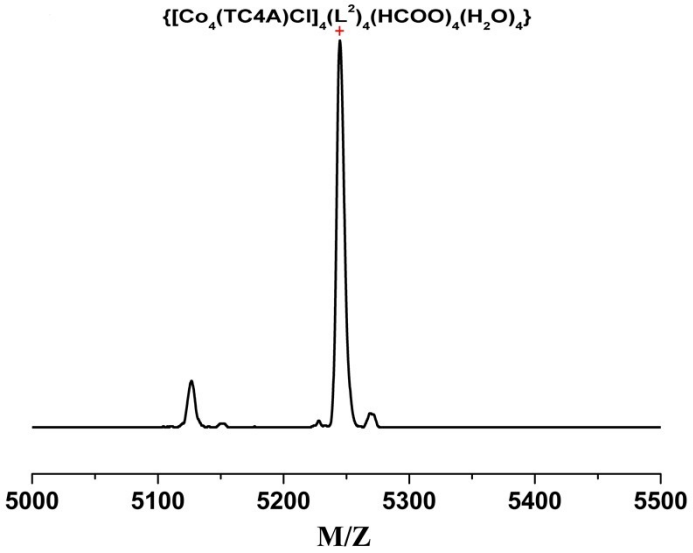

Fig. S9. MALDI-TOF mass spectrum of the resulting solutions presenting the feature peaks of $\{[Co_4(TC4A)Cl]_4(L^2)_4(HCOO)_4(H_2O)_4\}$ assembly in **CIAC-119**.

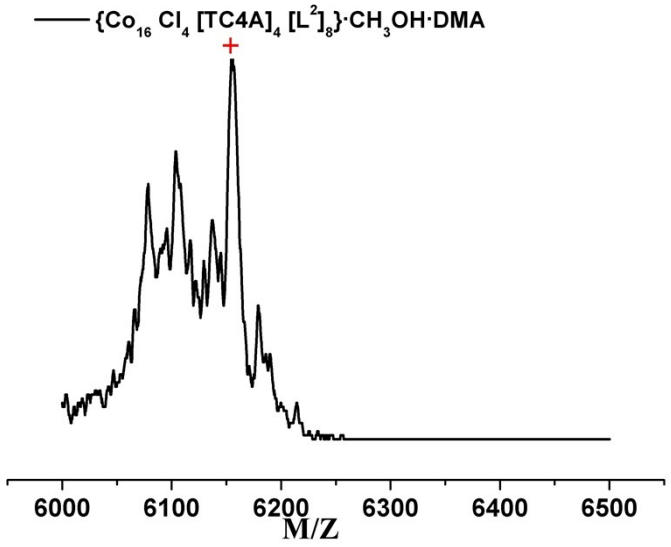

Fig. S10. MALDI-TOF mass spectrum of the resulting solutions presenting the feature peaks of $\{[Co_{16}\ Cl_4\ [TC4A]_4[L^2]_8\}$ assembly in **CIAC-120**.

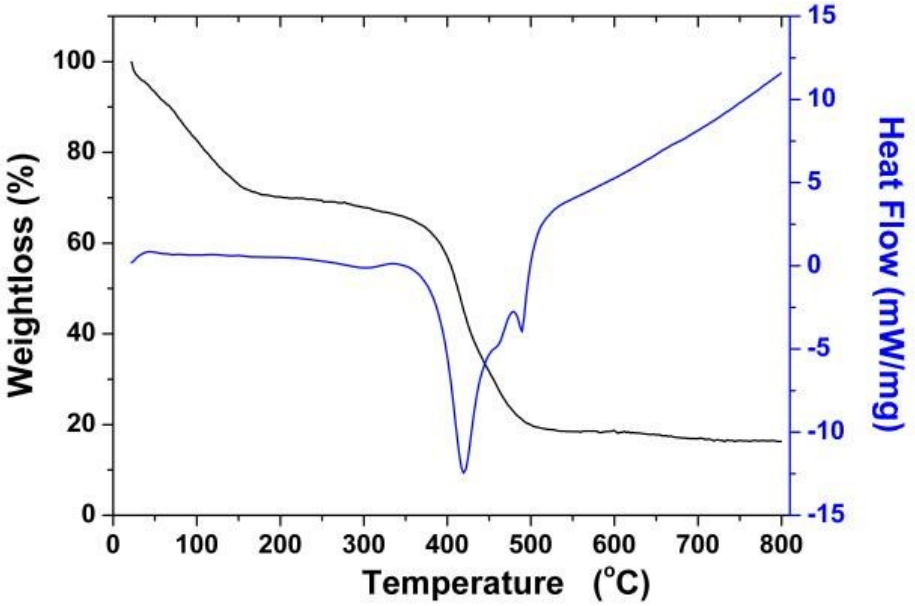

Fig. S11. TGA-DSC curves of **CIAC-117** exhibiting the weight loss in the temperature ranges 20-800 °C.

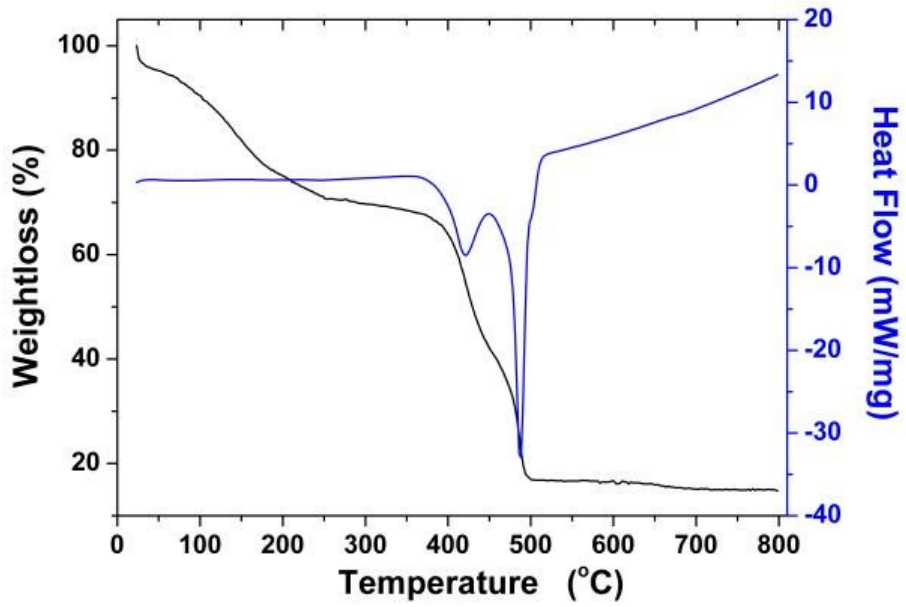

Fig. S12. TGA-DSC curves of **CIAC-118** exhibiting the weight loss in the temperature ranges 20-800 °C.

Fig. S13. TGA-DSC curves of **CIAC-119** exhibiting the weight loss in the temperature ranges 20-800 °C.

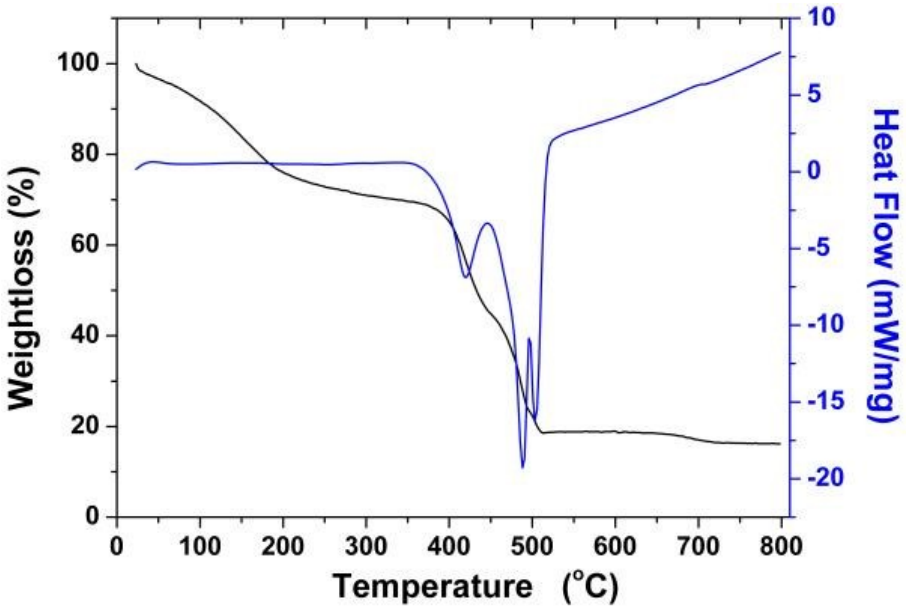

Fig. S14. TGA-DSC curves of **CIAC-120** exhibiting the weight loss in the temperature ranges 20-800 °C.

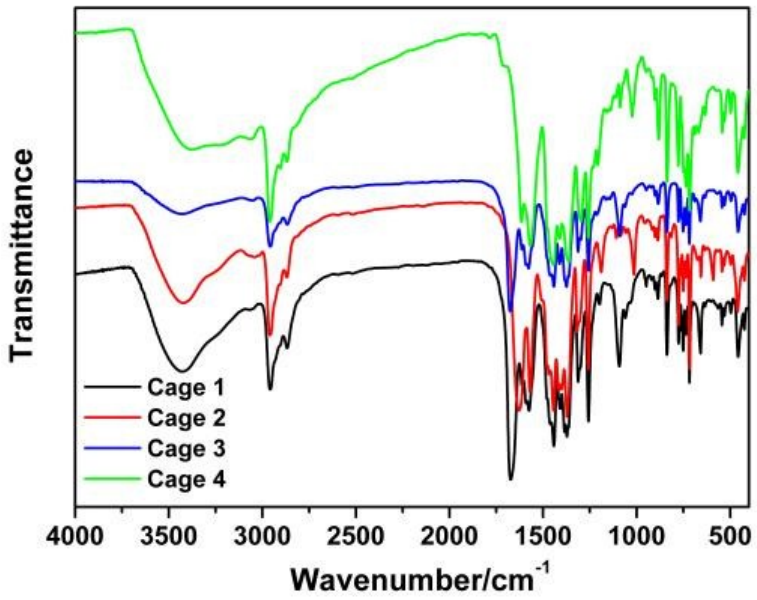

Fig. S15. FT-IR spectra of the compounds **CIAC-117- CIAC-120**.

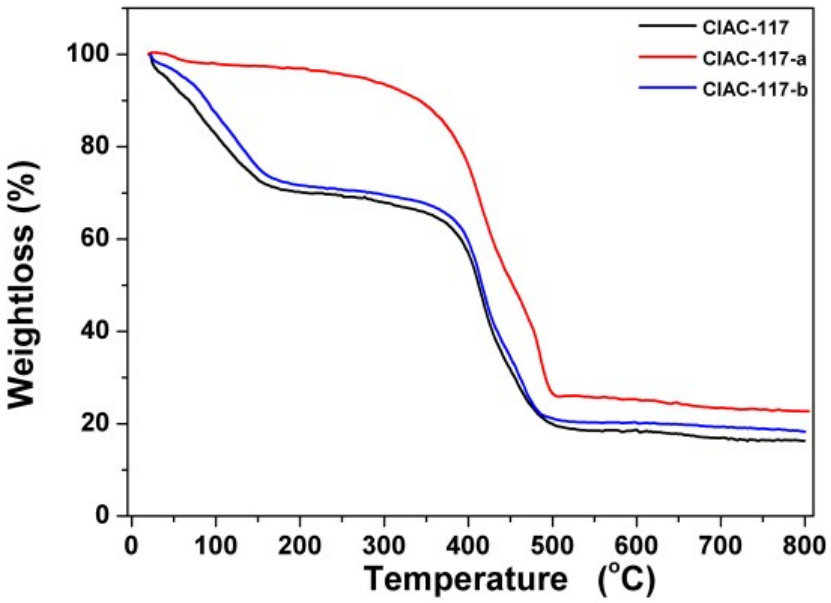

Fig. S16. TG curves of as-synthesized **CIAC-117**, **CIAC-117-a** and **CIAC-117-b**.

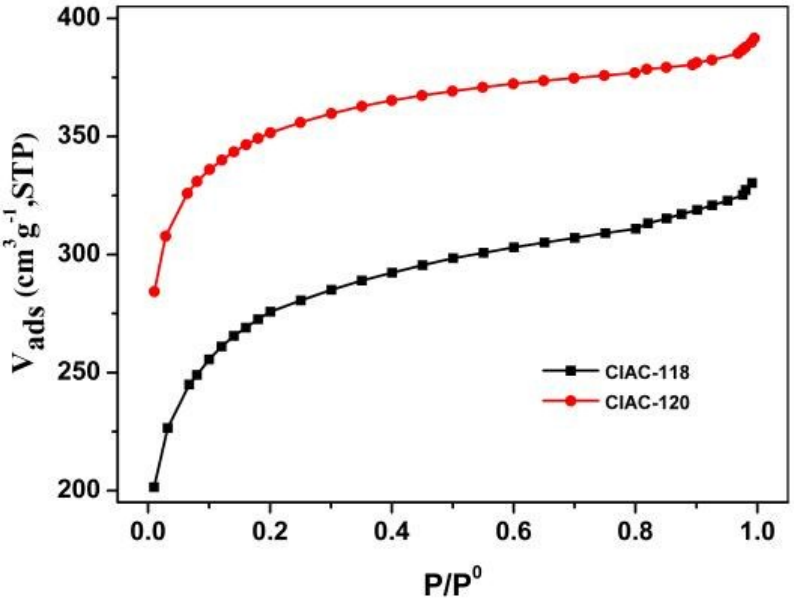

Fig. S17. N_2 adsorption isotherms at 77 K of **CIAC-118** and **CIAC-120**.

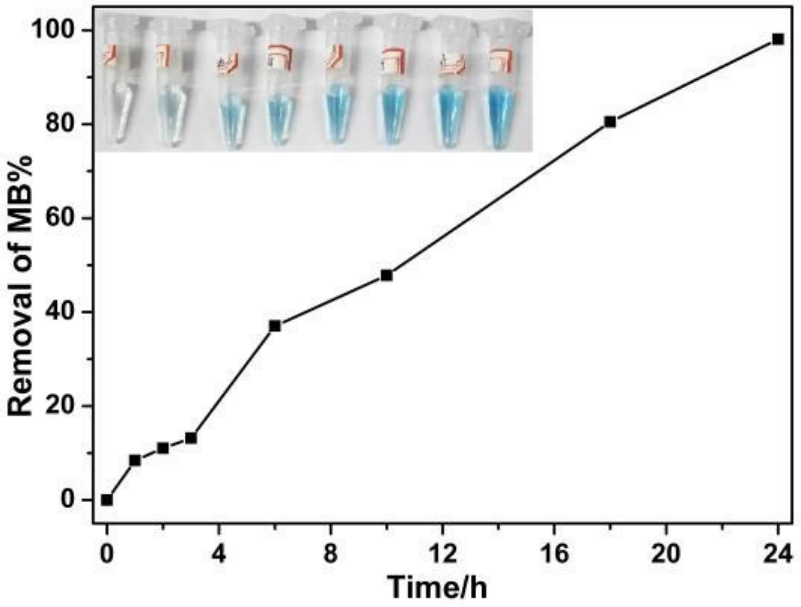

Fig. S18. Removal efficiency of MB over **CIAC-120**. The inset photos represent the color change of MB solutions upon adsorption by **CIAC-120**. Time increases in the order from the right to the left.

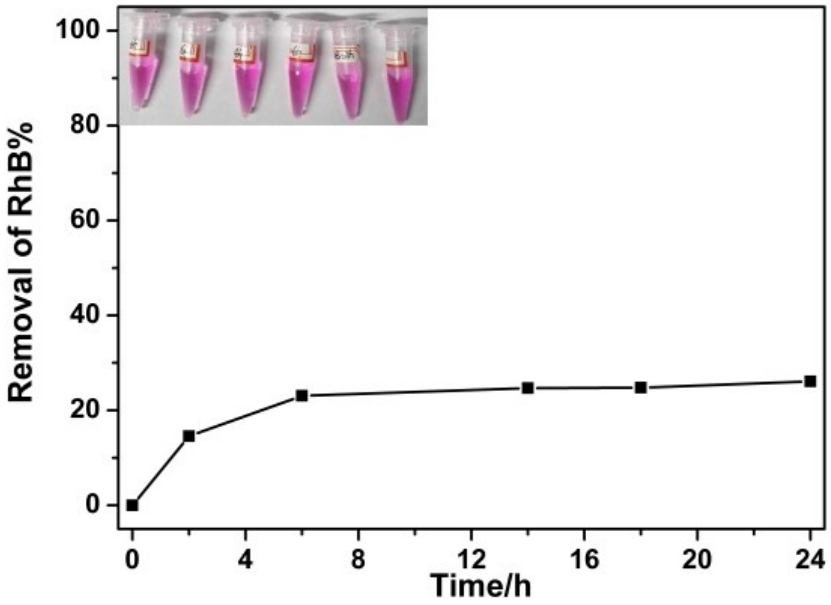

Fig. S19. Removal efficiency of RhB over **CIAC-120**. The inset photos represent the color change of RhB solutions upon adsorption by **CIAC-120**. Time increases in the order from the right to the left.

Fig. S20. Photographs of the color change of the mixed dyes MB/RhB solutions before and after adsorption experiments at given intervals with **CIAC-120**. Time increases in the order from the right to the left.

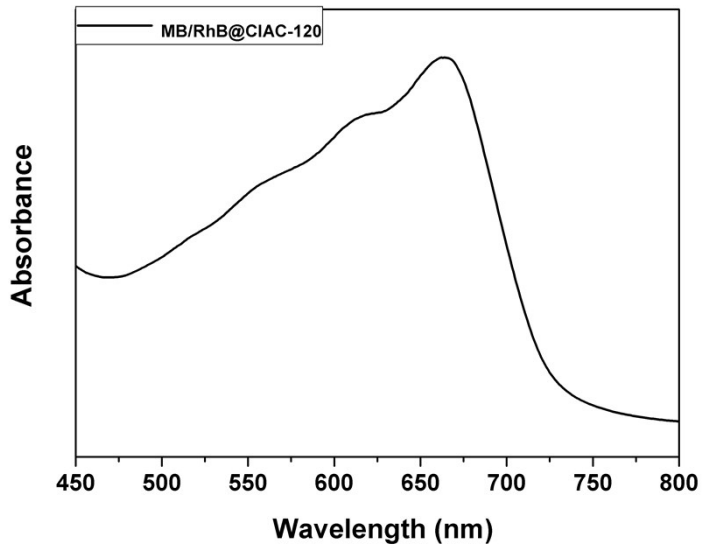

Fig. S21 Solid-state UV-Vis spectra of **MB/RhB@CIAC-120**.

After dye adsorption in a mixture of MB and RhB (both being of 10 mg/L) for 24 hours, the samples of MB/RhB@CIAC-120 were collected by filtration, washed with H_2O and CH_3OH for three times, respectively, and dried in air. Then the samples were analyzed by a solid-state UV-Vis spectrophotometer. The characteristic absorption peak of MB was observed, but the characteristic absorption peak of RhB was not obvious, which indicates that MB is selectively adsorbed and encapsulated in the crystalline material.

Table S1. Crystal data and structure refinement for compounds **CIAC-117-CIAC-120** without the involved solvent molecules.

	CIAC-117	**CIAC-118**	**CIAC-119**	**CIAC-120**
formula	$C_{216}H_{216}N_4O_{44}S_{16}Cl_4Co_{16}$	$C_{264}H_{232}N_8O_{48}S_{16}Cl_4Co_{16}$	$C_{216}H_{212}N_4O_{44}F_4S_{16}Cl_4Co_{16}$	$C_{264}H_{224}N_8O_{48}F_8S_{16}Cl_4Co_{16}$
formula wt	5169.81	5882.20	5241.43	6026.14
cryst. syst.	monoclinic	Tetragonal	monoclinic	Tetragonal
space group	C2/c	I 4/m	C2/c	I 4/m
a (Å)	42.516(2)	30.1630(3)	42.6717(11)	30.1442(3)
b (Å)	28.4143(14)	30.1630(3)	26.3547(7)	30.1442(3)
c (Å)	33.6347(17)	21.6122(4)	33.6116(9)	21.5579(5)
α (°)	90.00	90.00	90.00	90.00
β (°)	111.972(2)	90.00	113.5760(10)	90.00
γ (°)	90.00	90.00	90.00	90.00
V(Å^3)	37682(3)	19662.9(5)	34644.5(16)	19589.1(5)
Z	4	2	4	2
D_c/g cm^{-3}	0.909	0.994	1.003	1.021
μ / mm^{-1}	6.799	6.578	7.418	6.641
F(000)	10544	6024	10672	6152
total data	11444	4033	12358	4019
unique data	8868	3702	10743	3558
R_{int}	0.1214	0.0843	0.0613	0.0508
GOF	1.051	1.111	1.099	1.133
R1[a] [I > 2σ(I)]	0.0675	0.1102	0.0638	0.0857
wR2[b](all data)	0.1967	0.3110	0.1543	0.2780

[a] $R1 = \Sigma||F_0|-|F_c||/\Sigma|F_0|$; [b] $wR2=\{\Sigma[w(F_0^2-F_c^2)^2]/\Sigma[w(F_0^2)^2]\}^{1/2}$